



Investigation of fatigue and fracture characteristics for low-temperature metals considering the effects of various alloying components

Jeong Yeol Park¹ · Myung Hyun Kim^{1,2}

Received: 25 September 2019 / Accepted: 15 June 2020 / Published online: 25 June 2020
© International Institute of Welding 2020

Abstract

In the past few decades, low-temperature metals such as SUS304L, nickel alloys, and high-manganese steels have been widely used for liquefied natural gas (LNG) storage tanks to satisfy the structural integrity requirements at low temperature. Many researchers have conducted studies to characterize the fatigue and fracture performance of low-temperature metals. However, only a limited number of studies have considered the effects of various welding processes and consumables. This study addresses the fatigue and fracture performance of low-temperature metals while considering the effects of various alloying components. Moreover, we investigated the fatigue and fracture performance of various welding processes. Flux core arc welding (FCAW) was employed for both SUS304L and 9 wt.% nickel alloy steel, while tungsten inert gas (TIG) and shield metal arc welding (SMAW) were applied to SUS304L and 9 wt.% nickel alloy steel, respectively. Submerged arc welding (SAW) was employed for high-manganese steel. Fatigue and fracture tests were conducted according to ASTM E647 and BS 7448. The mechanical properties of the weld metals were systematically analyzed. SUS304L with FCAW exhibited excellent crack tip opening displacement (CTOD) and fatigue crack growth rate (FCGR). We also observed the microstructure of weld metals and discuss the mechanisms related to the fatigue and fracture performance in the parent and weld metals.

Keywords Mechanical properties · Fatigue crack growth rate (FCGR) · Crack tip opening displacement (CTOD) · Low-temperature metals · Alloying components

1 Introduction

To avoid serious environmental pollution, the International Maritime Organization (IMO) has recently reinforced regulations on nitrogen oxide (NO_x) and sulfur oxides (SO_x). In accordance with MARPOL Annex VI, the NO_x limit in Tier III and the global SO_x limit will be reduced from 3.5 to 0.5%, which will be effective in January 2020 [1]. This has led to increasing demands for liquefied natural gas (LNG) in China,

India, and the Middle East [2]. As the demand for LNG increases, more LNG carriers (LNGCs), floating liquefied natural gas (FLNGs), and very large gas carriers (VLGCs) are required.

The structural integrity of storage tanks is one of the most important issues in the construction of LNG carriers. In order to establish the structural integrity of storage tanks, the primary barrier is typically manufactured with low-temperature metals, as shown in Table 1. In general, commonly employed low-temperature metals such as Invar alloys, Al 5083, SUS304L, 9 wt.% nickel alloy, and high-manganese steels exhibit excellent fatigue performance at cryogenic temperature. Many studies have been carried out to investigate the fatigue and fracture performance of such metals.

Oh et al. [3] investigated the fatigue performance of low-temperature metals such as Invar alloy, Al 5038-O, 9 wt.% nickel alloy steel, and SUS304L. In particular, they quantitatively evaluated the improvement in fatigue performance of each low-temperature metal at cryogenic temperatures [3]. Hwang et al. [4] evaluated the low-cycle fatigue (LCF)

Recommended for publication by Commission XIII - Fatigue of Welded Components and Structures

✉ Myung Hyun Kim
kimm@pusan.ac.kr

¹ Department of Naval Architecture and Ocean Engineering, Pusan National University, Busan 609-735, South Korea

² International School of Ocean Science and Engineering, Harbin Institute of Technology, 92 West Dazhi Street, Nan Gang District, Harbin, China

Table 1 Operation temperature of low-temperature metals [3]

Min. design temp. (°C)	Metal	Application
–60	1.5% nickel steel	Storage tank in propane gas carriers
–65	2.25% nickel steel	
–90	3.5% nickel steel	Storage tanks in ethane gas carriers
–105	5% nickel steel	
–165	Al 5083-O, SUS304L, 9% nickel, & High-manganese steels	Storage tank in natural gas carriers

performance of 304-L stainless steel weldments to assess the fatigue life in the plastic strain region. The LCF results of weldments were found to exhibit similar tendencies in terms of the thickness [4].

Hyundai Heavy Industry (HHI) [5] assessed the fatigue and fracture performance of 9 wt.% nickel alloy steel. The fatigue performance satisfied the requirements of the fatigue design curves suggested by the IIW recommendations [6]. In terms of fracture toughness, the heat-affected zone (HAZ) has the lowest crack tip opening displacement (CTOD) value among 3 locations (HAZ, parent, and weld metals). Park et al. [7] investigated the fatigue crack growth rates (FCGRs) of nickel alloy steels while considering the nickel content. The material constant *C* in the Paris law associated with the FCGR of 9 wt.% nickel alloy steel was the highest among various nickel alloy steels. In addition, the slope of the relationship between the fatigue crack growth exponent, *m*, and the nickel content is increased as the temperature decreases.

Jeong et al. [8] evaluated the near-threshold FCGR of low-temperature metals such as high-manganese, SUS304, and 9 wt.% and 5 wt.% nickel alloy steels. High-manganese steels showed excellent near-threshold FCGRs at 25 °C and –100 °C compared to other low-temperature metals [8]. However, only a limited number of studies discuss the effects of alloying components on the fatigue and fracture behavior of low-temperature metals. Therefore, this study addresses these effects on the fatigue and fracture performance of the low-temperature metals such as SUS304L, 9 wt.% nickel alloy, and high-manganese steels. In addition, we investigate the fatigue and fracture performance with various welding processes.

2 Low-temperature metals

The chemical composition is very important for the fatigue and fracture performance of low-temperature metals. The

Table 2 Chemical composition of low-temperature metals

	C	Mg	P	N	S	Si	Cr	Ni	Mn	Mo
9% Ni	0.1	–	0.035	–	0.02	0.35	0.25	8.5–10	0.3–0.9	0.1
SUS304L	0.03	–	0.045	0.10	0.03	0.75	18–20	8–12	2.00	–
High Mn	0.45	–	0.02	–	0.03	0.41	3.57	–	26.81	–

Table 3 Applied welding processes and chemical composition of welding consumables

Classification	Materials	Welding processes	C	Mn	Ni	Cr	P	Etc.
9Ni-FC AWS ENiCrMo3T1-4	9% Ni	FCAW	0.02 0.10 max.	0.3 0.50 max.	66.0 58.0 min.	21 20.0–23.0	0.005 0.02 max.	Mo: 8.50, Nb: 3.40 Mo: 8.0–10.0 Nb: 3.15–4.15
9Ni-SM AWS ENiCrMO-6		SMAW	0.03 ≤0.10	2.5 2.00–4.00	69.9 ≥55.0	13.43 12.0–17.0	– ≤0.03	Mo: 7.00, Nb: 1.30 Mo: 5.0–9.0 Nb+Ta: 0.5–2.0
SUS-FC SUS-TI AWS E308LTX-X	SUS304L	FCAW TIG –	0.034 0.014 ≤0.04	1.52 1.51 ≤2.0	10.1 9.74 9.0–11.0	19.2 19.08 18.0–21.0	0.023 0.021 ≤0.03	S: 0.013, Si: 0.59 S: 0.003, Si: 0.40 S: ≤0.025 Si: ≤1.2
Mn-SA	High Mn	SAW	0.35–0.5	18–22	1–4	1.5–3.5	0.003	Mo, W

Table 4 Welding parameters

Classification	Materials	Welding processes	Current (A)	Voltage (V)
9Ni-FC	9% Ni	FCAW	170–180	27–28
9Ni-SM		SMAW	150–160	23–24
SUS-FC	SUS304L	FCAW	180–220	–
SUS-TI		TIG	250	26
Mn-SA	High Mn	SAW	790	34

Table 5 Information of welding procedure

Classification	Materials	Welding processes	Plate thickness	Joint configuration	Groove angle	Diameter of consumable
9Ni-FC	9% Ni	FCAW	20 mm	X groove	60°	1.2 mm
9Ni-SM		SMAW				3.2 mm
SUS-FC	SUS304L	FCAW	10 mm	X groove	–	–
SUS-TI		TIG				
Mn-SA	High Mn	SAW	20 mm	K groove	35°	3.2 mm

mechanical properties and the fatigue and fracture performance are strongly affected by the contents of P, S, Cr, and Si. Toughness is adversely affected by high contents of P and S, and high contents of Si and Cr are known to decrease the grain size while increasing the amount of retained austenite [9]. This study considers SUS304L, 9 wt.% nickel alloy (9% Ni), and high-manganese (high Mn) steels in tensile, CTOD, and FCGR tests. The chemical compositions of the metals are summarized in Table 2.

3 Test preparation

Five welding consumables manufactured with various chemical compositions were compared to evaluate the fatigue and fracture performance in welds. Welding consumables are denoted by the acronyms in Table 3. In addition, Tables 4 and 5 present the welding parameters related to the heat input of

each process and information of welding procedure, respectively.

A servo-hydraulic testing machine (Instron Model 8803) was used for the tensile, fatigue, and fracture tests. The machine has a maximum load capacity of ± 500 kN. The COD gauge length is 10 mm, and the travel length is 4 mm. The test machine and COD gauge are presented in Fig. 1.

Tensile tests were conducted according to ASTM E8 [10]. The mechanical properties were measured, including the yield and tensile strengths, elongation, and reduction of area [10]. The tensile test specimens were manufactured according to Part 6.4 in ASTM E8. The geometry of a standard round bar specimen is illustrated in Fig. 2.

The CTOD test is a common fracture mechanics test that measures the resistance of a material to fracture. The CTOD test was conducted with CT specimens according to BS 7448, as illustrated in Fig. 3 [11]. The thickness of test specimens is 10–20 mm, the width is 40–60 mm, and the height is 48–72 mm, depending on the thickness of the materials.

Fig. 1 Test equipment. **a** Servo-hydraulic test machine. **b** COD gauge

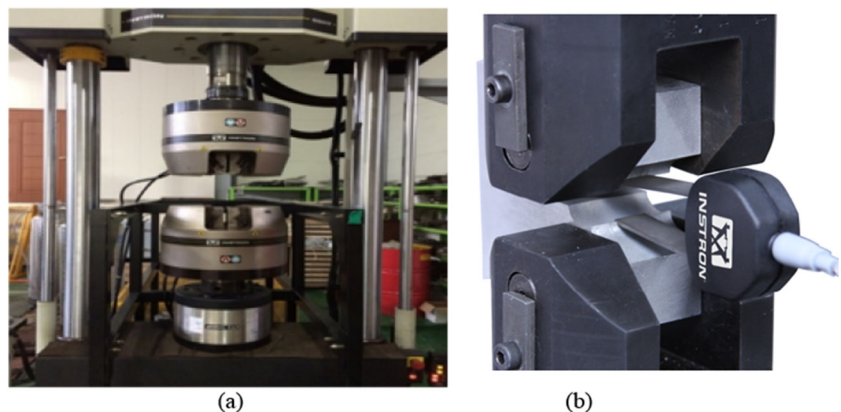
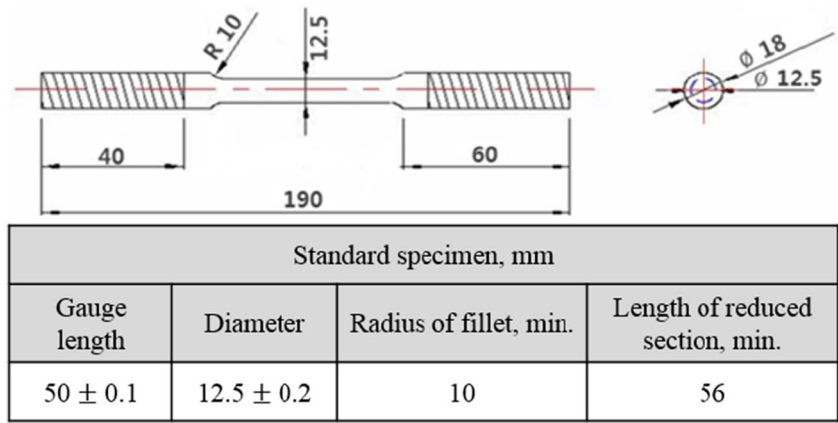


Fig. 2 Standard round tension test specimen in ASTM E8 [10]



The FCGR test was conducted according to ASTM E647 [12]. The test specimens for SUS304L, 9% Ni steel, and high Mn-steel are 10–20 mm in thickness, 50–80 mm in width, and

60–96 mm in height. Figures 3 and 4 present the typical geometry of a 9% Ni test specimen. The test specimens for the other metals have similar geometry except for the dimensions.

Fig. 3 Dimensions of CT specimen (9% Ni)

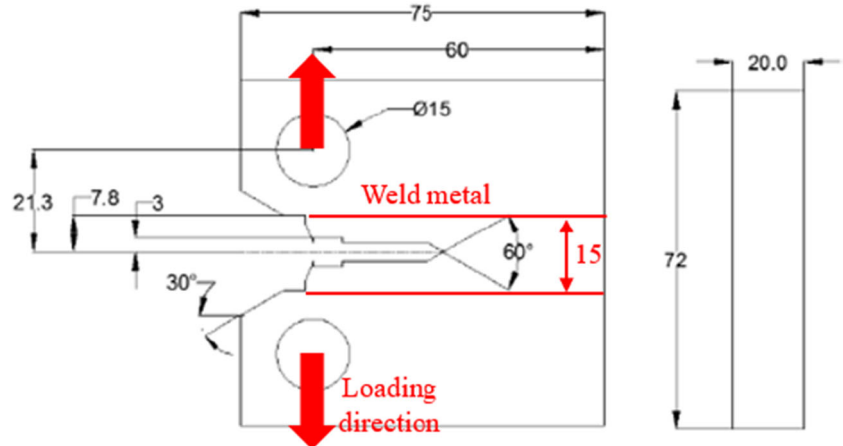
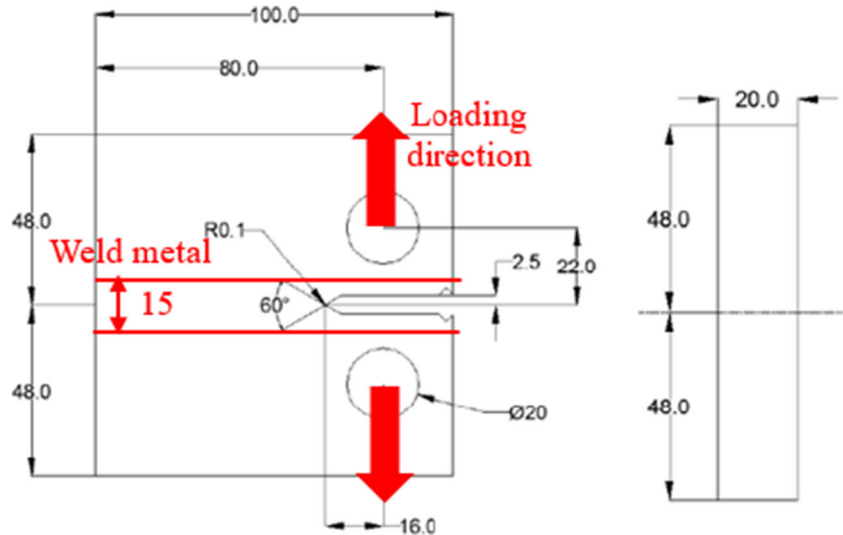


Fig. 4 Dimensions of FCGR specimen (9% Ni)



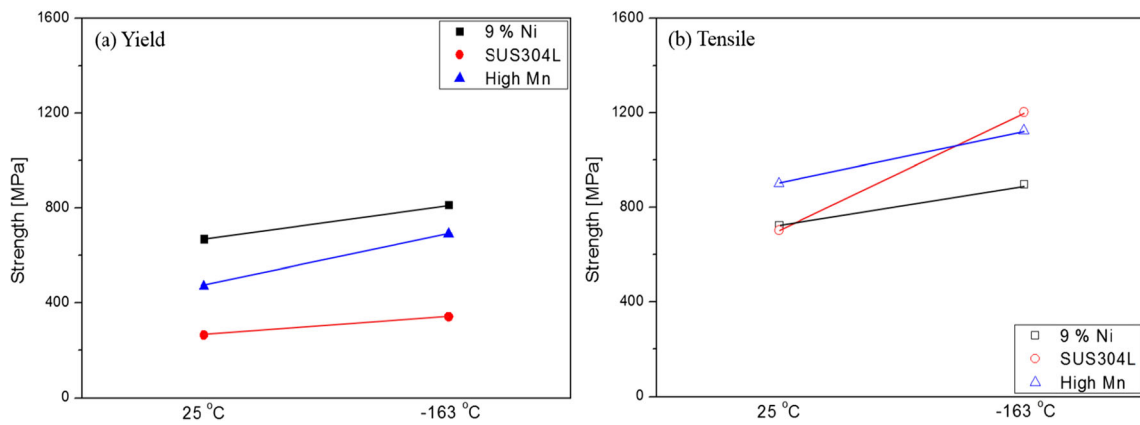


Fig. 5 Comparison of tensile properties of parent metals. a Yield strength. b Tensile strength

Table 6 Requirement of mechanical properties

	YS (MPa)	TS (MPa)
9% Ni	≥ 490	640 ~ 840
SUS304L	≥ 175	450 ~ 700
High Mn	≥ 400	800 ~ 970

4 Results and discussion

4.1 Parent metals

4.1.1 Tensile properties

Figure 5 shows the yield strength (σ_{YS}) and tensile strength (σ_{TS}) of the parent metals from the tensile test results [13]. In addition, Table 6 summarizes the requirement for mechanical properties of parent metals. In comparison of Table 6, the mechanical properties of three parent metals satisfy the steel grade requirements. High-Mn steel exhibits excellent tensile strength at room temperature. It is well known that the tensile

strength increases with the manganese content [14]. The high-Mn steel had the highest carbon content among the three parent metals considered. Therefore, the increase in tensile strength can be explained by the high carbon content [9]. Despite the excellent tensile strength, the weakness of high-Mn steel is the relatively low yield to tensile strength ratio [15]. There have been some studies to increase the yield strength in high-Mn steel [15]. The tensile properties of SUS304L exhibit a noticeable variation at cryogenic temperature compared to other metals.

4.1.2 Fracture toughness

CTOD tests for parent metals were carried out three times for the parent metals at both room and cryogenic temperatures, and the results are shown in Fig. 6. The CTOD of SUS304L is the highest at room temperature compared to the other two metals. In addition, the CTOD values of SUS304L and high manganese steel are similar. According to Mertinger et al. [16], increasing the chromium contents is known to increase the fraction of the retained austenite.

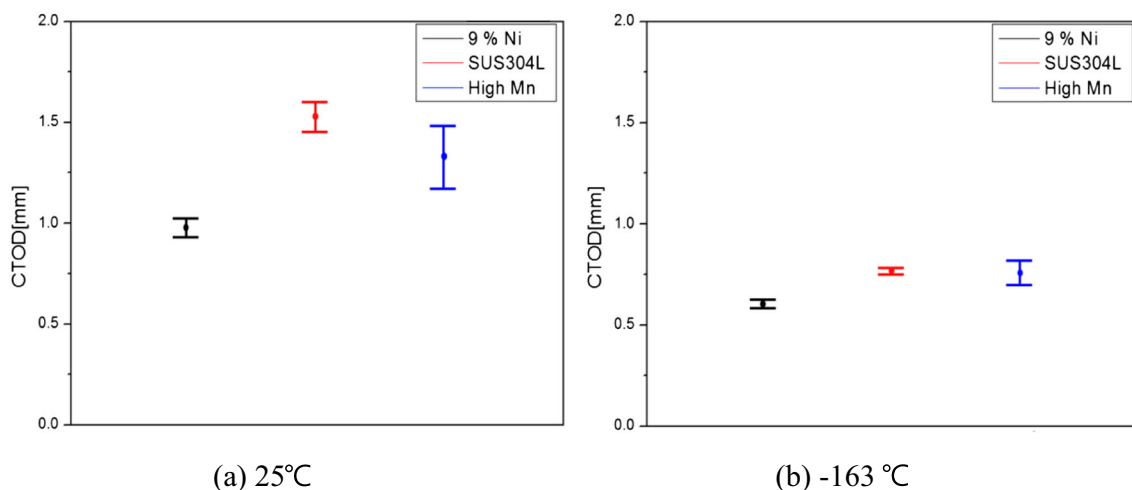


Fig. 6 CTOD values of parent metals: a 25 °C and b -163 °C

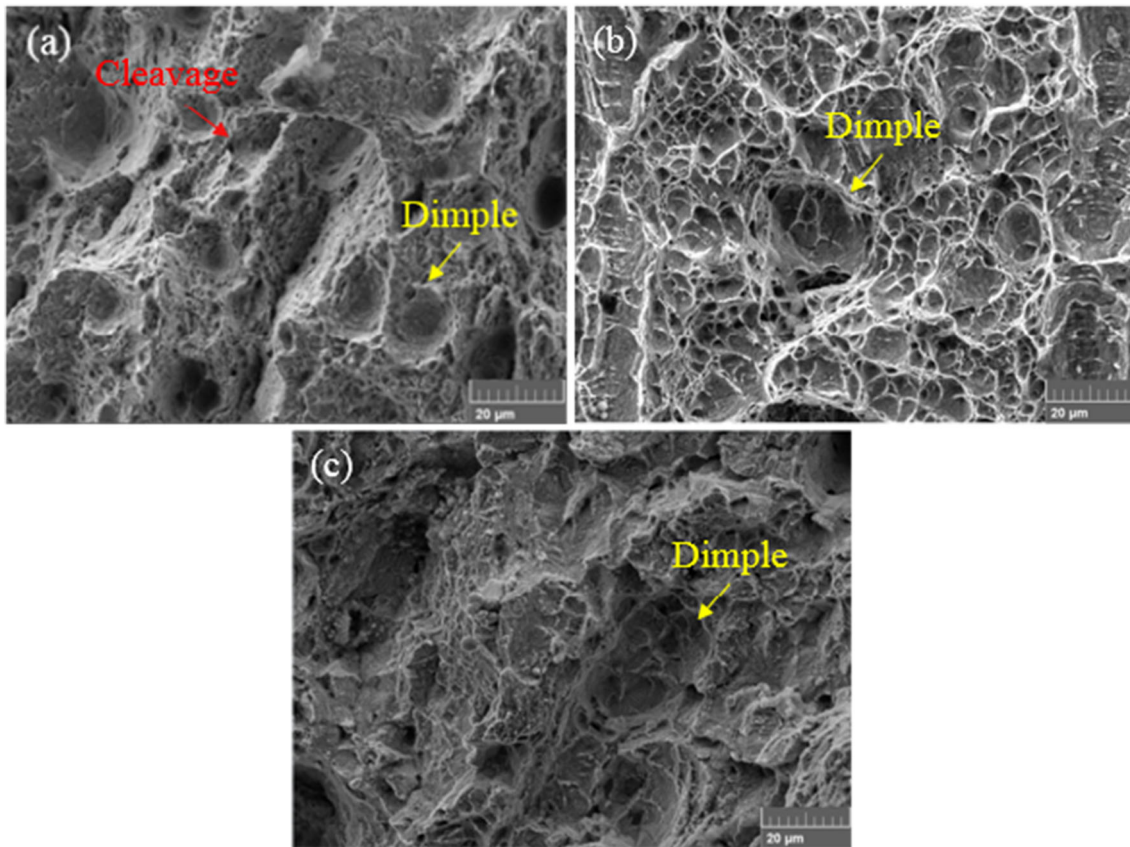


Fig. 7 Fracture surface in low-temperature metals after CTOD test at $-163\text{ }^{\circ}\text{C}$: **a** 9% Ni, **b** SUS304L, and **c** high Mn. The SEM images were obtained from the front of the fatigue pre-crack tip

Based on the microstructure analysis, the dimple structure of each low-temperature metal was examined, as shown in Fig. 7. At cryogenic temperature, the dimple size was the smallest for SUS304L, followed by high-Mn and 9% Ni steels. The dimple fracture mode of SUS304L can explain the higher toughness, while the dimple structure of 9% Ni exhibits a quasi-cleavage fracture mode.

4.1.3 Fatigue crack propagation

Figure 8 compares the FCGRs of the parent metals. The material constant m in the Paris equation is fixed at 3.0 to compare it with the FCGR value in BS7910 [17]. All FCG curves are presented in terms of the stress intensity factor (SIF) range of 20 and 50 $\text{MPa}\sqrt{\text{m}}$.

FCGR showed a different tendency from the yield strength. The FCGR of all parent metals tended to decrease as the temperature decreased. In addition, the FCGR of 9% Ni steel was greater than that of SUS304L and high-Mn steels. SUS304L exhibits the slowest FCGR behavior among the metals, which is attributed to the higher silicon content decreasing the grain size [18].

Figure 9 presents the fatigue striation observed in the parent metals at room temperature. The striation spacing is one of the criteria used for the assessment of fatigue crack retardation. The

9% Ni steel had the largest striation spacing among the metals, which suggests that faster fatigue crack growth will occur.

4.2 Weld metal

4.2.1 Tensile properties

Figure 10 shows the mechanical properties of weld metals [19]. At room temperature, the tensile strength of the Mn-SA

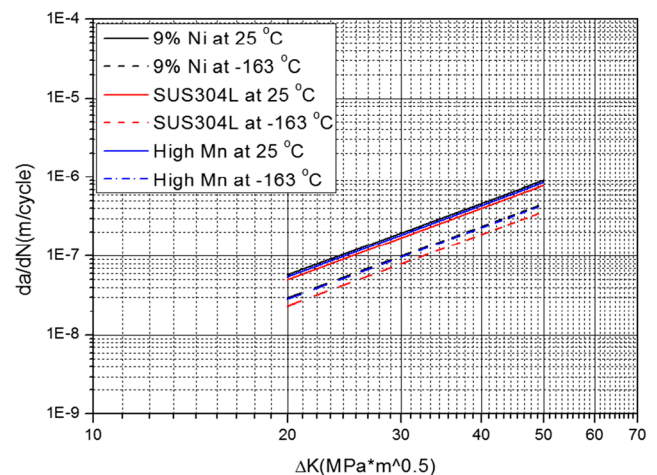


Fig. 8 da/dN - ΔK curves of parent metals

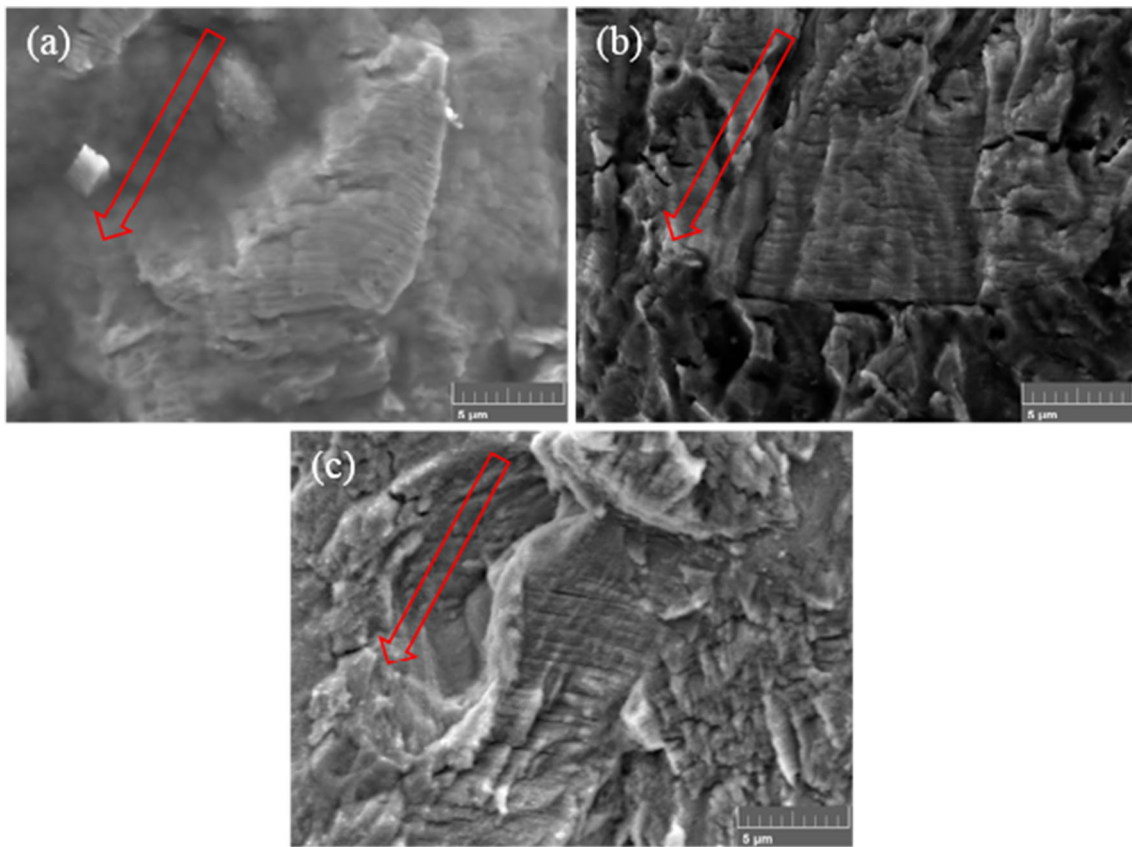


Fig. 9 Fracture surface of low-temperature metals after FCGR test at 25 °C: **a** 9% Ni, **b** SUS304L, and **c** high Mn. Red arrows: direction of fatigue crack. The SEM images were obtained from the front of the fatigue pre-crack tip

is the highest among the five weld metals. The increased tensile strength is attributed to the higher chromium content of up to 3.0 wt.% [20]. The tensile strengths of SUS-FC and SUS-TI are higher than those of the other weld metals at cryogenic temperature. Moreover, SUS-FC and SUS-TI exhibit drastic increases in the tensile strength at cryogenic temperature. It is estimated that the mechanical properties of SUS304L are substantially influenced by the secondary hardening [21].

The secondary dendrite arm spacing (SDAS) was investigated to provide further insight into the tensile behavior. Figure 11 compares the SDAS of the five weld metals, and the values are summarized in Table 7. The SDAS of SUS-TI is the largest, while Mn-SA has the smallest value. The SDAS tends to decrease as the tensile strength increases [22]. Therefore, the strong increase in tensile strength can be explained by the low SDAS.

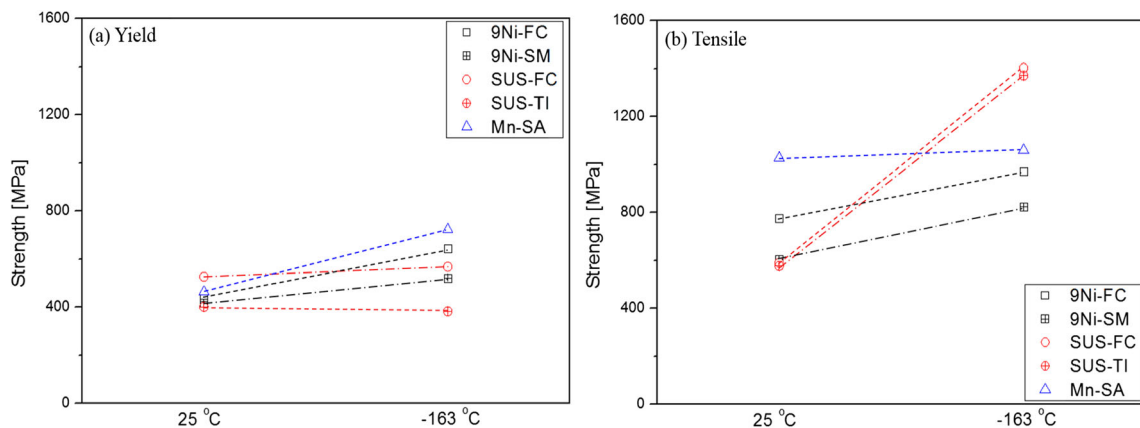


Fig. 10 Comparison of mechanical properties for weld metals. **a** Yield strength. **b** Tensile strength

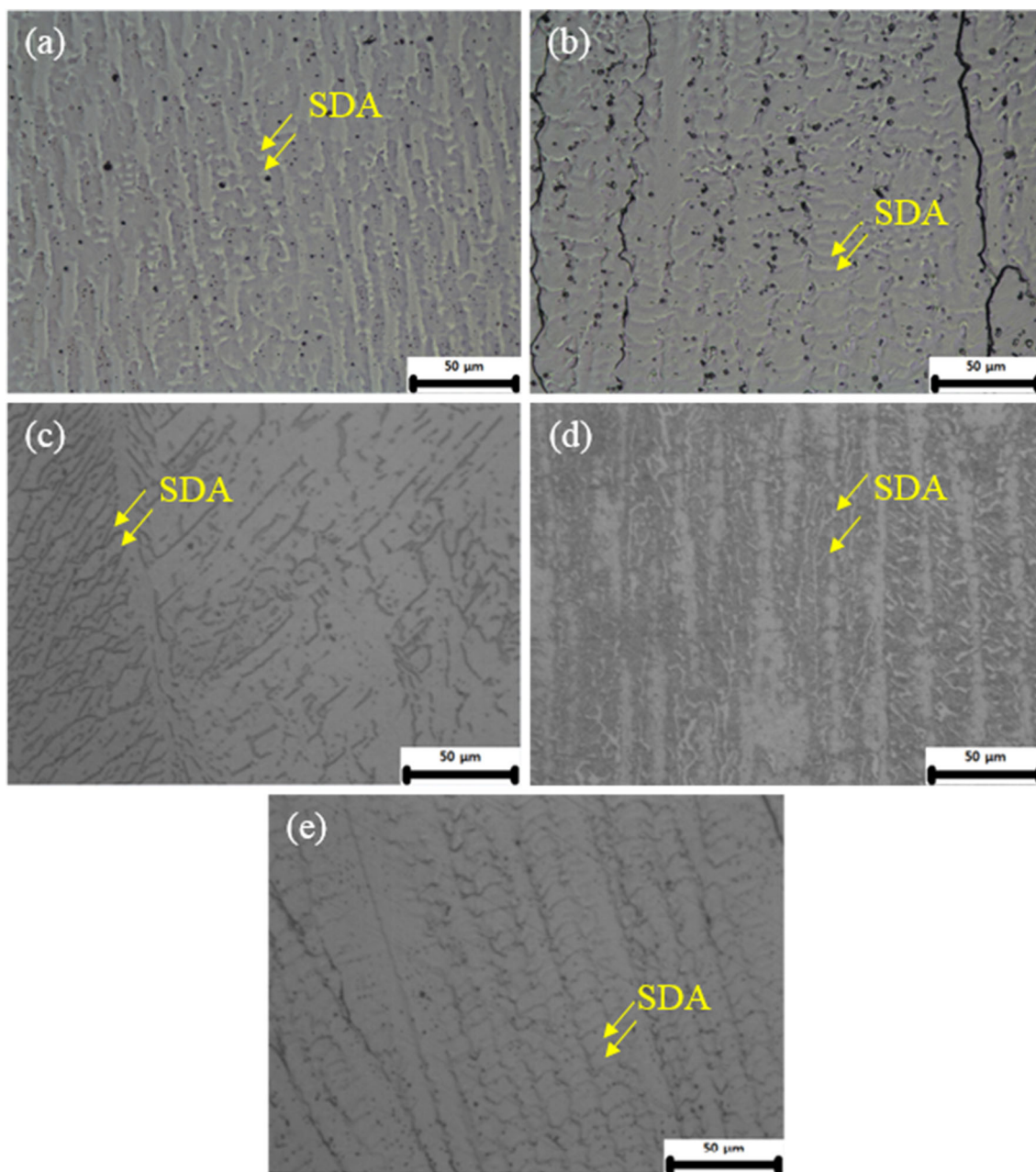


Fig. 11 Secondary dendrite arm spacing of five weld metals: **a** 9Ni-FC, **b** 9Ni-SM, **c** SUS-FC, **d** SUS-TI, and **e** Mn-SA. Yellow arrows: secondary dendrite arm

4.2.2 Fracture toughness

The CTOD values of the weld metals were measured three times for each metal with various welding processes and consumables, and the results are compared in Fig. 12. All five weld metals satisfy the minimum

CTOD requirement by DNVGL at both room and cryogenic temperatures [23]. In addition, there was a large variation of CTOD values in SUS-FC and SUS-TI at cryogenic temperature. According to the reference paper, the increase in sigma phase has an adverse effect on fracture toughness [24]. In addition, Gow and Harder

Table 7 Secondary dendrite arm spacings of five weld metals

	9Ni-FC	9Ni-SM	SUS-FC	SUS-TI	Mn-SA
Secondary dendrite arm spacing (μm)	21.18	26.75	27.72	36.30	19.26

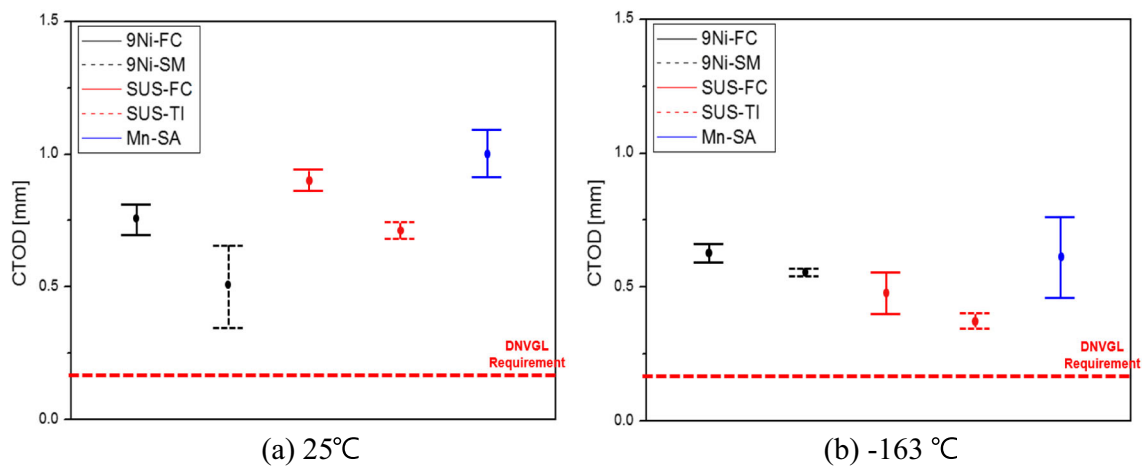


Fig. 12 CTOD values of weld metals: a 25 °C and b - 163 °C

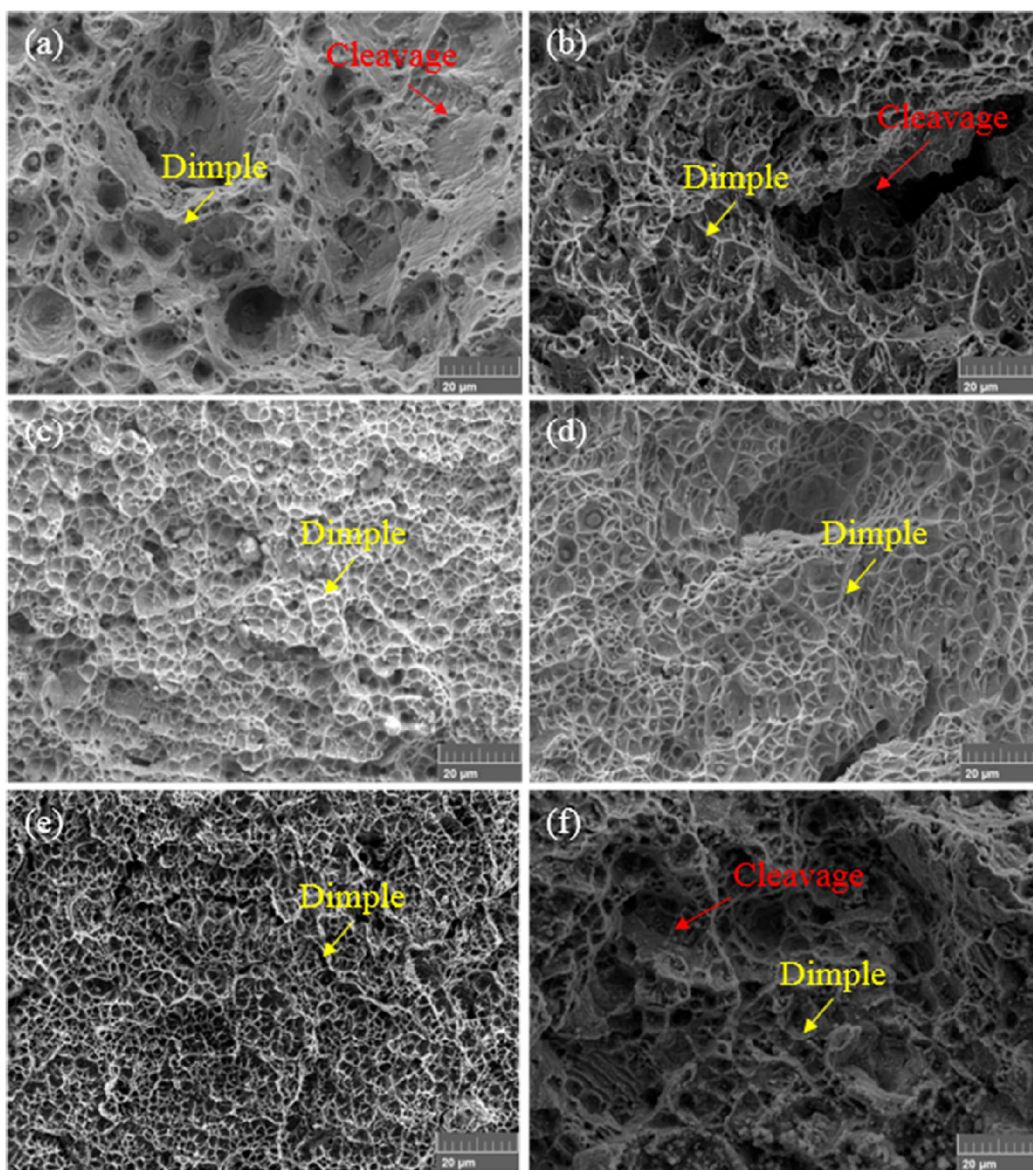
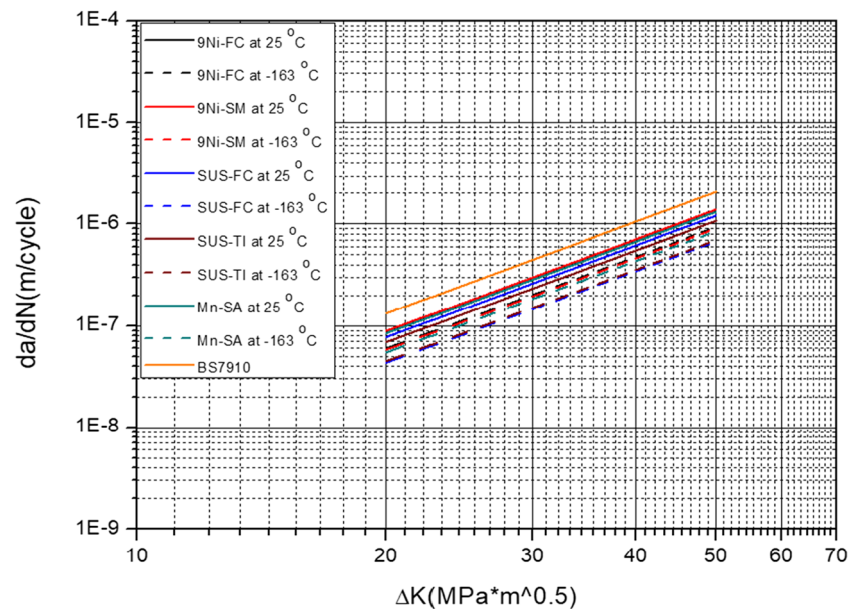


Fig. 13 Fracture surface in weld metals after CTOD test at - 163 °C (d): a 9Ni-FC, b 9Ni-SM, c SUS-FC, d SUS-FC at 25 °C, e SUS-TI, and f Mn-SA. The SEM images were obtained from the front of the fatigue pre-crack tip

Fig. 14 $da/dN-\Delta K$ curves in weld metals.



[25] suggested that if ratio factor > 1.7 , the sigma phase can precipitate in stainless steels.

$$\text{Ratio factor} = \frac{\%Cr - 16 * \%C}{\%Ni}$$

In cases of SUS-FC and SUS-TI, the ratio factors are 1.84 and 1.93, respectively. Therefore, it is estimated that the fracture toughness of SUS-FC and SUS-TI at cryogenic temperature is affected by sigma phase.

The Mn-SA has the highest CTOD value at room temperature. According to Havel [20], the content of molybdenum is typically increased to stabilize the austenite in high-Mn steel. In this study, the welding consumable used for high-Mn steel includes molybdenum. As the temperature decreases, the CTOD values of weld metals in 9% Ni and high-Mn steel become higher than that of SUS304L. The contents of sulfur and phosphorus were negligible in the welding consumables of 9% Ni and high-Mn steel.

The dimple structures of weld metals are illustrated in Fig. 13. The dimple size of SUS-TI is the smallest, and that of SUS-FC was sensitive to the temperature changes. Therefore, the variation of the dimple size with temperature can account for the CTOD values at cryogenic temperature.

4.2.3 Fatigue crack propagation

Figure 14 compares the FCGRs in weld metals. SUS-FC and SUS-TI exhibit slower fatigue crack growth rates at both room and cryogenic temperatures. The silicon content influences the decrease in FCGR due to the presence of martensite [26]. One major observation is that the FCGRs of SUS-FC and SUS-TI exhibit significant variation with temperature compared to the

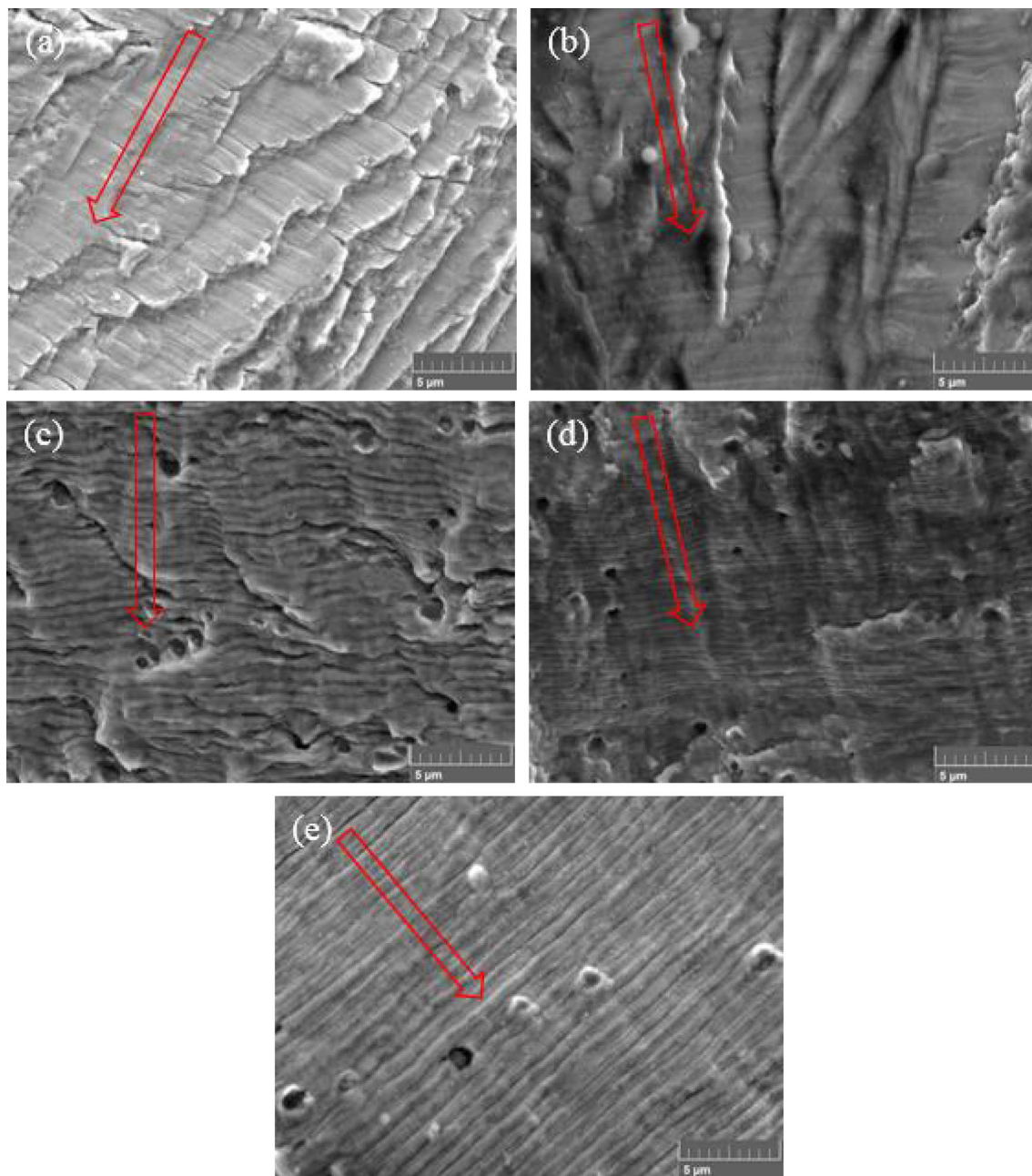
other weld metals. In the case of the weld metal in SUS304L, the austenite changes into martensite when the temperature decreases [27]. The martensitic transformation that occurs at the tip of fatigue cracks in SUS304L appears to reduce the FCGR significantly [28].

We observed the striation in weld metals at room temperature to investigate the microstructure effects on FCGR, as shown in Fig. 15. SUS-TI has the lowest striation spacing. FCGR tends to decrease as the striation spacing decreases. According to the SEM images, the FCGR results can be reasonably explained by the observed striation spacing, indicating slower fatigue crack growth with lower striation spacing.

5 Summary and conclusion

We investigated the fatigue and fracture performance of the low-temperature metals SUS304L, 9% Ni, and high-Mn steel while considering the effects of different alloying components. In addition, microstructure analysis was performed on five weld metals to investigate the fatigue and fracture performance. The important observations are summarized as follows:

- The tensile strength of high-Mn steel exhibits excellent tensile strength at room temperature in the parent and weld metals. The tensile strength is affected by the amounts of manganese, carbon, and chromium. In the case of the weld metal, the low SDAS can explain the substantial increase in tensile strength. In addition, the tensile strength of SUS304L has significant variation with the temperature decrease as shown in Fig. 5b. The increase in tensile strength of 9% Ni, high Mn, and SUS304 are 21%,



(e) Mn-SA

Fig. 15 Fracture surface of weld metals after FCGR test at 25 °C: **a** 9Ni-FC, **b** 9Ni-SA, **c** SUS-FC, **d** SUS-TI, and **e** Mn-SA. The SEM images were obtained from the front of the fatigue pre-crack tip

42%, and 20%, respectively. Therefore, the tensile strength of SUS304L is strongly increased at cryogenic temperatures compared to the other two steels. It is estimated that the mechanical properties of SUS304L are substantially influenced by secondary hardening.

- The CTOD values of SUS304L are the highest at room temperature compared to the other two metals. At cryogenic temperature, CTOD values of SUS304L and high manganese steel are similar. In case of FCC austenite

steels, it can be explained that higher chromium content is known to increase the fraction of the retained austenite. The dimple fracture mode of SUS304L can explain the higher toughness than that of 9% Ni steel, where the dimple structure showed a quasi-cleavage fracture mode.

- The minimum CTOD values of SUS-FC and SUS-TI weld metal were lower than those of other three weld metals as the temperature decreased. The decrease in fracture toughness at low temperature is influenced by the

contents of sulfur and phosphorus. Mn-SA has the highest CTOD value at room temperature. In high-Mn steel, the amount of molybdenum is increased to stabilize the austenite. As the temperature decreases, the CTOD values of weld metals in 9% Ni and high-Mn steel became higher than that of SUS304L. The contents of sulfur and phosphorus were negligible in the welding consumables of 9% Ni and high-Mn steel. The dimple size of SUS-TI is the smallest among weld metals. Therefore, the variation in the dimple size with temperature can account for the CTOD values at cryogenic temperature.

- SUS304L exhibits the slowest FCGR behavior among the low-temperature metals, which is attributed to the higher silicon content, which in turn plays a role in reducing the grain size. Furthermore, 9% Ni steel had the largest striation spacing compared to SUS304L and high-Mn, which suggests that faster fatigue crack growth will occur.
- The fatigue crack growth rates of SUS-FC and SUS-TI weld metals was the slowest at both room and cryogenic temperatures. The silicon content influences the decrease in FCGR due to the presence of martensite. FCGRs of SUS-FC and SUS-TI exhibit strong variation with temperature. The martensitic transformation that occurs at the tip of a fatigue crack in SUS304L significantly reduces the FCGR. SUS-TI exhibits the lowest striation spacing among the five weld metals. According to the SEM images, FCGR results can be reasonably explained by the striation spacing, indicating slower fatigue crack growth with lower striation spacing.

Acknowledgments This work was supported by the National Research Foundation of Korea (NRF) grant funded by the Korea government (MSIT) through GCRC-SOP (No. 2011-0030013). This work was also supported by the National Research Foundation of Korea (NRF) grant, which is also funded by the Korea government (MOE) (NRF-2017R1D1A1B03035811).

References

1. Revised MARPOL Annex VI (2016) Amendments to the annex of the protocol of 1997 to amend the international convention for the prevention of pollution from ships. International Maritime Organization. <https://www.imo.org>
2. Overview Report (2015) An overview of the world LNG market and Canada's potential for exports of LNG. Canadian Association of Petroleum Producers. Calgary, Alberta
3. Oh DJ et al (2015) Investigation of fatigue performance of low temperature alloys for LNG storage tanks. *J Mech Eng Sci*:1–15
4. Hwang JH, Oh DJ, Lee DY, Chun MS, Kim MH (2016) Low cycle fatigue performance of 304L stainless steel weldments. *Journal of Welding and Joining* 34(3):47–51
5. Hyundai Heavy Industries (2012) Mechanical and fatigue properties at room and cryogenic temperatures for 9% Ni steel. HHI Technical report
6. A. Hobbacher (2007) Recommendations for fatigue design of welded joints and components. IIW document XIII- 2151-07/XV-1254-07
7. Park JY et al. (2016) Fatigue crack propagation characteristics of 3.5 to 9 wt% nickel steels for low temperature applications. *Proceeding of OMAE*. OMAE2016-54740:1-7
8. Jeong DH, Lee SG, Yoo JY, Lee JS, Kim S (2015) Comparative studies on near-threshold fatigue crack propagation behavior of high manganese steels at room and cryogenic temperatures. *Mater Charact* 103:28–36
9. Kang KJ (2012) *Engineering materials*. Bookshill. ISBN 9788955267808
10. ASTM (2015) Standard test method for tension testing of metallic materials. ASTM E8
11. BS (1991) Method for determination of K_{Ic} critical CTOD and critical J values of metallic materials. BS 7448
12. ASTM (2013) Standard test method for measurement of fatigue crack growth rates. ASTM E647
13. Shim HJ et al (2007) Evaluation of the fatigue strength and the mechanical properties for cargo containment system in LNG ship. *Journal of KSME*:15–20
14. Bohuslav M et al (2010) The effect of Mn and Si on the properties of advanced high strength steels processed by quenching and partitioning. *Mater Sci Forum* 654-656:94–97
15. Song SW, Lee JH, Lee T, Lee CS (2017) Effect of the amount and temperature of prestrain on tensile and low-cycle fatigue properties of Fe-17Mn-0.5C TRIP/TWIP steel. *Materials Science & Engineering A* 696(1):493–502
16. Mertinger V et al. (2015) Effect of Cr content on the TWIP behavior in Fe-Mn-Cr steels. *International Conference on Martensitic Transformations* 2(3): 673-676. Bilbao, Spain
17. BS (2013) Guide to methods for assessing the acceptability of flaws in metallic structures, BS 7910
18. Anya CC, Baker TN (1989) The effect of silicon on the grain size and the tensile properties of low carbon steels. *Mater Sci Eng* 118: 197–206
19. Yuri T, Ogata T, Saito M, Hirayama Y (2000) Effect of welding structure and d-ferrite on fatigue properties for TIG welded austenitic stainless steels at cryogenic temperatures. *Cryogenic* 40:251–259
20. Havel D (2017) Austenitic manganese steel; a complete overview. Technical Report. Columbia Steel Casting Co., Inc.
21. Kim JH, Kim SK, Kim MH, Lee JM (2014) Numerical model to predict deformation of corrugated austenitic stainless steel sheet under cryogenic temperatures for design of liquefied natural gas insulation system. *Mater Des* 57:26–39
22. Askeland DR et al. (2005) *The science and engineering of materials* 5th edition. CENGAGE Learning, ISBN 0534553966
23. DNV GL Maritime (2015) Fabrication and testing of offshore structures
24. Lippold JC et al. (2005) *Welding metallurgy and weldability of stainless steels*. John Wiley & Sons, Inc. ISBN 0471473790
25. Gow JT et al (1942) Balancing the composition of cast 25 per cent chromium-12 per cent nickel type alloys. *Transactions of the American Society for Metals* 30:855–935
26. Drumond J, Girina O, da Silva Filho JF, Fonstein N, de Oliveira CAS (2012) Effect of silicon content on the microstructure and mechanical properties of dual-phase steels. *Metallography, Microstructure, and Analysis* 1(5):217–223
27. Qiu H et al (2013) Thermal stability of retained austenite in Cr–Ni weld metals at low temperatures. *Mater Sci Technol* 29(5):597–597
28. Mei Z, Morris JW (1990) Influence of deformation-induced martensite on fatigue crack propagation in 304-type steels. *Metall Trans A* 21(A):3137–3152

Publisher's note Springer Nature remains neutral with regard to jurisdictional claims in published maps and institutional affiliations.